

Synchronized ion acceleration by ultraintense slow light

A. V. Brantov,^{1,2} E. A. Govras,^{1,2} V. F. Kovalev,^{2,3} and V. Yu. Bychenkov^{1,2}

¹*P. N. Lebedev Physics Institute, Russian Academy of Science, Moscow 119991, Russia*

²*Center for Fundamental and Applied Research, Dukhov Research Institute of Automatics (VNIIA), Moscow 127055, Russia*

³*Keldysh Institute of Applied Mathematics, Russian Academy of Sciences, Moscow 125047, Russia*

An effective scheme of synchronized laser-triggered ion acceleration and the corresponding theoretical model are proposed for a slow light pulse of relativistic intensity, which penetrates into a near-critical-density plasma, strongly slows, and then increases its group velocity during propagation within a target. The 3D PIC simulations confirm this concept for proton acceleration by a femtosecond petawatt-class laser pulse experiencing relativistic self-focusing, quantify the characteristics of the generated protons, and demonstrate a significant increase of their energy compared with the proton energy generated from optimized ultrathin solid dense foils.

With the rapid development of laser technology, several acceleration concepts using short relativistically intense laser pulses are applied for generating high-energy ions [1, 2]. Most mechanisms of laser-triggered ion generation are tailored to a forward acceleration of ions from solid targets, but a new trend has recently appeared in this field based on using low-density targets [3, 4], which could be related to advanced materials such as aerogels, nanoporous carbon, etc. The hope in using such targets are that they may increase the energy of the accelerated ions compared with solid targets, particularly when ions are accelerated by lasers that are now available with ~ 1 PW power. One of the challenging ways for accelerating ions up to ~ 1 GeV by such lasers is ion wake-field acceleration [5, 6], but this is a difficult task for existing high-power laser systems because heavy particles cannot be pre-accelerated and trapped by the wake field as easily as electrons can [7, 8].

For an effective acceleration in a rare plasma, similarly to electron wake-field acceleration, ions must be pre-accelerated up to a velocity close to the speed of light. Based on simplified 1D and 2D numerical simulations, several two-stage schemes for ion acceleration have been proposed [9–12] to test the idea using an additional target (thin foil or micro-droplets) to pre-accelerate ions in the radiation-pressure-dominated regime [13]. These ions can then be trapped and accelerated in a gas plasma. For the proposed scenario to be viable, an Exawatt-class laser is required. The further development in this direction involved the laser snowplow effect in a near-critical density plasma, where the electrostatic potential generated by the laser pulse accelerates and reflects ions [5, 14, 15] similarly to collisionless electrostatic shock acceleration [16]. Specifically, a near-critical-density plasma, which reduces the laser group velocity, was proposed [15] for a second stage of accelerating ions initially pre-accelerated from a thin target by a circularly polarized super-Gaussian pulse. Based on the simulation results, a proton acceleration to an energy of hundreds of MeV was reported. It is important that the effect of relativistically induced transparency plays a key role in ion acceleration with a near-critical density plasma [14].

A pulse of intense slow light can trap slow or even at-rest ions in its ponderomotive sheath potential, which acts as a snow plow on electrons and accelerates ions. But a laser pulse with a group velocity significantly less than the speed of light cannot accelerate ions to a high energy ~ 1 GeV until the group velocity itself starts to increase during pulse propagation. In this letter, we propose a new scheme for ion acceleration by a femtosecond laser pulse from a low-density target with an electron density near the threshold of relativistic transparency. The key point of this scheme is the capability for the laser pulse first to slow and then to increase its group velocity monotonically with the propagation distance. This is an effective way to accelerate ions by a laser ponderomotive field on the up-going pulse similarly to electron acceleration on the down-going pulse ramp [17]. The monotonic increase of the pulse group velocity makes ions achieve a synchronized acceleration by slow light (SASL). We also present an analytic model and 3D PIC simulations that demonstrate how SASL works when the increase of the pulse group velocity during the propagation of a femtosecond petawatt-class laser pulse in a near-critical-density plasma is due to relativistic self-focusing. Schemes of something similar to particle-field synchronization have been proposed by Katsouleas [18] (accelerated electrons and wake field in a rare plasma with a decreasing density) and by Bulanov et al. [19] (accelerated ions and electromagnetic field in the radiation-pressure regime).

A relativistic laser pulse can propagate in a plasma with the electron density $n_e/\gamma n_c < 1$, where n_c is the electron critical plasma density and γ is the electron gamma factor. The group velocity $v_g = c\sqrt{1 - n_e/\gamma n_c}$ (c is the speed of light) of the light pulse inside the plasma should be small for effective loading and trapping of the ions in a self-consistent ponderomotive sheath. This is possible only in a rather narrow range of target densities, $n_e \sim \gamma n_c$, which slow a laser pulse and allow only the very top of the pulse with a sufficiently large intensity for relativistic self-transparency to propagate. For a given laser intensity, we should correspondingly expect a substantial selectivity of the target density, and this is

an expected specific feature of the acceleration scenario that we discuss.

When the front of a laser pulse hits an overdense target ($n_e > \gamma n_c$), it penetrates the target to a skin depth $\sim c\sqrt{\gamma}/\omega_{pe}$ and pushes electrons by the ponderomotive force F_p . This force quickly moves electrons deeper into the target creating an electron density spike at the pulse front until F_p is balanced by the charge separation electric force (see, e.g., [20, 21]), which roughly corresponds to the electron equilibration $eE \sim F_p = -\nabla\Phi$. The slower the pulse propagation is, the more accurate the estimate $eE = F_p$. To describe the SASL mechanism qualitatively, we adopt this equality and the widely used estimates $\Phi = m_e c^2 \gamma$ and $\gamma = \sqrt{1 + a^2(x, t)/2}$ for the ponderomotive potential and gamma factor, where $a = 0.85 \sqrt{I[10^{18} \text{ W/cm}^2] \lambda^2 [\mu\text{m}]}$ is the normalized amplitude of the laser vector potential. Initially, the characteristic scale length of the pulse intensity is the skin depth. It increases in time (as laser pulse intensity increases) and reaches a value $\sim c/\omega_0$, when the target becomes transparent for the near-peak intensity. The pulse starts propagating inside the target with a small group velocity $v_g \ll c$. In some specific cases, the group velocity can increase as the light penetrates deeper into the plasma, for example, as a result of relativistic self-focusing or a monotonic decrease of the target density from front to back. The ponderomotive electric sheath, which propagates in the plasma with the same group velocity, i.e., $\Phi = m_e c^2 \sqrt{1 + a^2(x - v_g t)/2}$, can trap some ions. If the rate of ponderomotive ion acceleration is close to the rate of the laser pulse acceleration, then the ions gain energy very efficiently. To justify this, we consider the equations of motion for a test ion (a proton, for definiteness) accelerated in the traveling ponderomotive sheath

$$\frac{dp}{dt} = -\frac{d}{d\xi}\Phi(\xi), \quad \frac{dx}{dt} = v = \frac{p}{\sqrt{1 + p^2}}, \quad (1)$$

where the coordinates x and $\xi(x, t) = x - tv_g(t)$ are normalized to the characteristic pulse spatial width σ . The time t , the velocities v and v_g , the momentum p , and the sheath potential Φ are respectively normalized to σ/c , c , $m_p c$, and $m_e c^2/\rho$ ($\rho = m_e/m_p = 1/1836$).

System of equations (1) describes a nonlinear oscillator and allows finite and infinite motion. Finite motion corresponds to ion reflection from the sheath as for acceleration by a collisionless shock wave [22]. For example, in the nonrelativistic limit $p \ll 1$, system (1) has a well-known solution in the case of a constant group velocity $v_g = v_{g,0}$. If the initial proton velocity p_0 is less than $v_{g,0}$, i.e., the parameter $\delta v = p_0 - v_{g,0} < 0$ and $\Phi_{\max} = \rho\sqrt{1 + a_0^2/2} > (\delta v)^2/2$ (cf. [15]), then the proton is reflected by the ponderomotive potential and attains the velocity $2v_{g,0} - p_0$. In the case of an accelerating pulse, i.e., a time-dependent group velocity $v_g(t)$,

the proton after being reflected can be caught by the pulse and reflected again. Each reflection increases the proton momentum in accordance with the instantaneous pulse velocity. These multiple reflections significantly accelerate the ion if it is in phase with the group velocity increase. We call this the SASL case. The opposite case of infinite motion corresponds to the absence of any ion reflection from the potential.

As an example of system (1), we consider a linearly increasing group velocity $v_g(t) = v_{g,0} + w_0 t$ in the nonrelativistic case $p \ll 1$. The corresponding analytic solution $\xi(t)$ is given in quadrature by the expression

$$t - t_0 = \pm \int_{\xi_0}^{\xi} \frac{dz}{\sqrt{\dot{\xi}_0^2 + 2(\Phi(\xi_0) - \Phi(z)) - 4w_0(z - \xi_0)}}, \quad (2)$$

where $\xi_0 = \xi(t_0)$ and $\dot{\xi}_0 = \dot{\xi}(t_0)$. Equation (2) in general form describes the ion motion starting at the instant t_0 from the position corresponding to $(\xi_0, \dot{\xi}_0)$. In the case of finite (oscillatory) motion, there are two return points in the pulse reference frame where $\dot{\xi} = 0$. In the laboratory reference frame, one of the return points corresponds to the maximum distance of the ion from the sheath (the point with the maximum coordinate ξ), and the second return point is the electrostatic sheath reflection point. The direction of ion motion from one return point (or the initial point corresponding to $t_0 = 0$, $\xi_0 = x_0$, $\dot{\xi}_0 = \delta v$) to the other defines the proper sign choice in Eq. (2).

To illustrate the obtained analytic solution given by Eq. (2), we present phase plots for the case of a Gaussian spatial profile of the ponderomotive electric field. Figure 1 shows the phase portraits for an ion that starts from $x_0 = 3$ with $\delta v = 0.01$ and is accelerated by an electrostatic sheath with $a_0 = 60$. The ion momentum is constrained by the value 0.5, when the nonrelativistic solution given by Eq. (2) becomes inapplicable. Figure 1

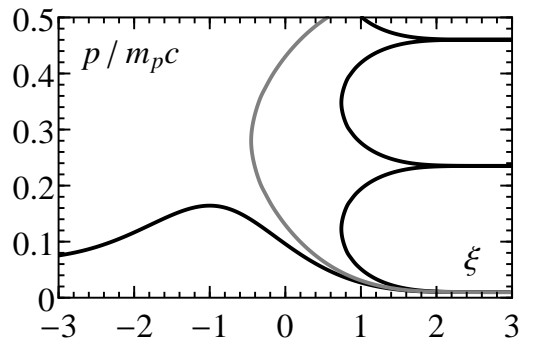


FIG. 1. Phase space for an ion starting from $x_0 = 3$ with $\delta v = 0.01$. The gray curve ($w_0 \approx 0.028$) separates the finite and infinite regimes illustrated by the examples $w_0 = 0.001$ (at the right) and $w_0 = 0.004$ (at the left) ($w_0 = 0.004$). The laser amplitude is $a_0 = 60$.

clearly demonstrates ion oscillations with multiple reflections from the pulse (SASL) for a sufficiently small pulse

acceleration w_0 , which allows an effective energy increase. The existence of two roots of the equation $\xi = 0$ defines a restriction on the pulse acceleration w_0 for which SASL is allowed:

$$w_0 \leq \frac{1}{2(x_0 - \xi_*)} \left[\Phi(\xi_*) - \Phi(x_0) - \frac{(\delta v)^2}{2} \right], \quad (3)$$

where the value ξ_* is defined from the solution of the equation

$$\Phi(\xi_*) - \Phi(x_0) = \frac{(\delta v)^2}{2} + (\xi_* - x_0)\Phi'(\xi_*). \quad (4)$$

For a given w_0 , we can find the domain of initial values $(x_0, \delta v)$ satisfying the SASL condition. Correspondingly, there is a maximum value of w_0 above which a synchronized ion-pulse motion is impossible. The dependence of the maximum pulse acceleration $\max(w_0)$ on the maximum laser pulse amplitude is shown in Fig. 2. The steep

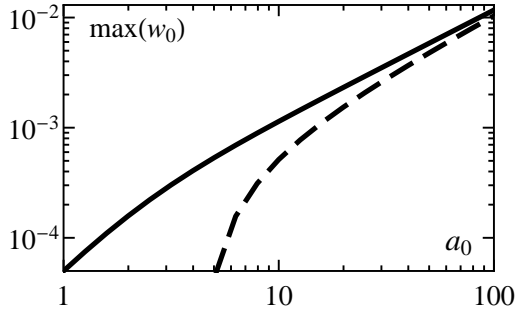


FIG. 2. Maximum pulse acceleration above which a synchronized ion-pulse motion is impossible for $\delta v = 0$ (solid curve) and $\delta v = \pm 0.05$ (dashed curve).

increase of $\max(w_0)$ with the laser field amplitude for sufficiently high $|\delta v|$ (i.e., $\delta v = \pm 0.05$; see the dashed curve in Fig. 2) in fact demonstrates the existence of the SASL threshold, i.e., $(\delta v)^2/2 = \Phi_{\max} - \Phi(x_0)$. The highest pulse acceleration is allowed only for protons initially at rest in the pulse reference frame, $\delta v = 0$.

From the first integral of Eq. (2), $\xi^2/2 - \xi_0^2/2 = \Phi(\xi_0) - \Phi(\xi) - 2w_0(\xi - \xi_0)$, we can estimate the proton energy increase. For protons initially at rest, the proton energy evolves as $\varepsilon = 2w_0(vt - x) + \Phi(\xi_0) - \Phi(\xi)$. In average, an ion moves together with the laser pulse and has a constant acceleration $x \sim w_0 t^2$, which results in an ion energy increase as $w_0^2 t^2$. We note this time dependence coincides with that for a Coulomb explosion of a plane target, which yields the maximum possible energy gain. But such a rapid energy gain is only in the nonrelativistic limit.

The nonrelativistic solution of system (1) can describe ion acceleration only for $\varepsilon \ll m_p c^2$, while the SASL can in principle yield a much higher ion energy. But for a linear time dependence of v_g , the relativistic nonlinearity in system (1) sooner or later breaks the SASL. The test ion

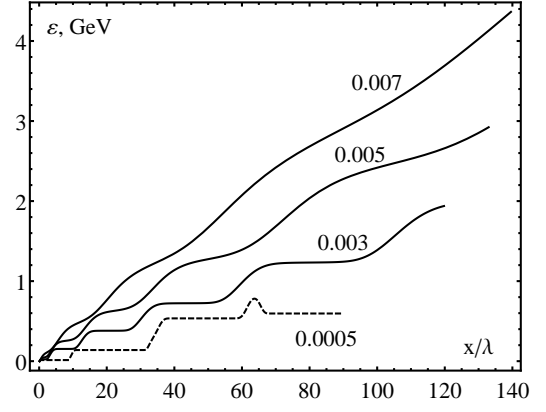


FIG. 3. The proton energy gain for $x_0 = 1$ and $p_0 = 0$ versus the propagation length for the ponderomotive potential characterized by $a_0 = 60$ and $v_g = w_0 t / (1 + w_0 t)$, where $w_0 = 0.003, 0.005, 0.007$ (the numbers near the curves). The dashed curve shows the energy gain for $a_0 = 60$ and $v_g = 0.0005t$.

acceleration decreases, and the ponderomotive potential of the laser pulse overcomes the ions. This occurs after three consecutive reflections from the sheath and is illustrated by the bump on the dashed line in Fig. 3. To describe the relativistic regime more accurately, we must take the natural saturation of the group velocity at the speed of light into account. We present the corresponding illustration in Fig. 3 as a result of solving system (1) numerically for the saturating group velocity $v_g = w_0 t / (1 + w_0 t)$, which shows continuous particle acceleration up to relativistic energies. The average energy of accelerated protons increases almost linearly with the propagation distance. Certainly, such a theoretical illustration cannot claim to be a proof of the new approach, but it at least vividly highlights the possible SASL advantage.

Other physical effects accompanying the laser pulse propagation, for example, pulse depletion, deformation of the pulse shape, violation of the ideal electron equilibration $eE \sim F_p$, complicate the theoretical model. They might degrade the theoretical estimates of the ion energy gain, but the basic principle of the SASL should remain. To confirm this, we performed 3D PIC simulations of proton acceleration by short (the FWHM pulse duration is 30 fs), tightly focused (the FWHM transverse size is 4λ) Gaussian laser pulses using the code MANDOR [23]. The laser intensities in the focal spot were $I = 5 \times 10^{20}$ W/cm² and $I = 5 \times 10^{21}$ W/cm², which correspond to the respective laser energies 3 J ($a_0 = 19.1$) and 30 J ($a_0 = 60$) for $\lambda = 1 \mu\text{m}$. The laser pulse was focused on the front side of a thin CH₂ plasma target, which consists of electrons, hydrogen ions, and fully ionized carbon ions (C⁶⁺). The target densities were decreased from the solid mass density of CH₂ (1.1 g/cm³), which corresponds to $n_e = 200n_c$ to the density 5.5 mg/cm³ ($n_e = n_c$). The target thickness l was varied from 3 nm to 10 μm .

Several runs with different target thicknesses were performed for each target density. The simulation results are presented in Fig. 4, which confirms the existence of an optimal target thickness in each case. Using a laser pulse

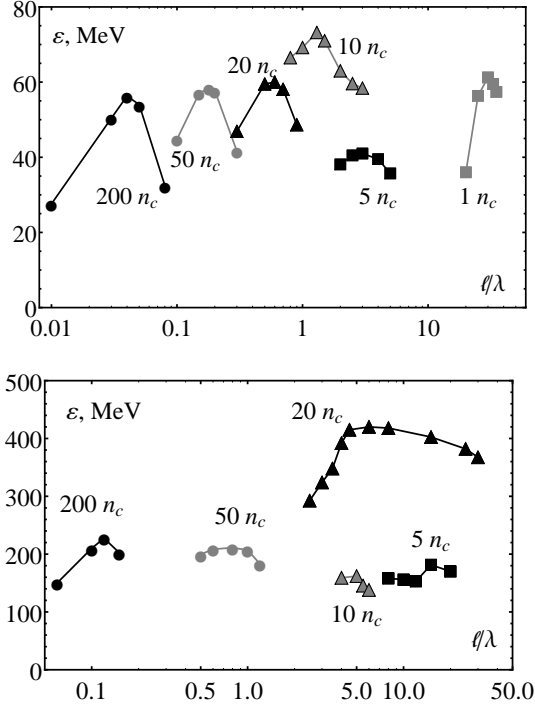


FIG. 4. Maximum proton energy versus target thickness for an electron target density of $200n_c$ (black points), $50n_c$ (gray points), $20n_c$ (black triangles), $10n_c$ (gray triangles), $5n_c$ (black squares), and n_c (gray squares) and for laser energies of 3 J (top panel) and 30 J (bottom panel).

with an energy of 3 J does not effectively synchronize the proton acceleration and laser pulse group velocity increase for any density, although there is a small proton energy increase (up to 30%). Proton acceleration by a petawatt-class laser with an energy of 30 J is more effective. For a target with an optimal density of $20n_c$, a significant increase of the maximum proton energy was found. For such a density, the front wing of the laser pulse does not penetrate into the target, but the near-peak intensity does penetrate and propagates inside the plasma with an increasing group velocity (the solid curve in the top panel of Fig. 5), which can be roughly approximated as $v_g = c(0.04 + 0.0045\omega t)$ (the dashed line in the top panel of Fig. 5). The laser-induced electrostatic sheath field corresponds well to the Gaussian-shape potential with $a_0 = 100$ and $\sigma = 2\omega/c$ (the dashed curve in the bottom panel of Fig. 5). For these parameter values, the increase of the pulse group velocity is sufficiently small ($w_0 = 0.009$), which is favorable for an effective trapping of the protons in the ponderomotive potential (cf. Fig. 2). The protons gain significant energy as a

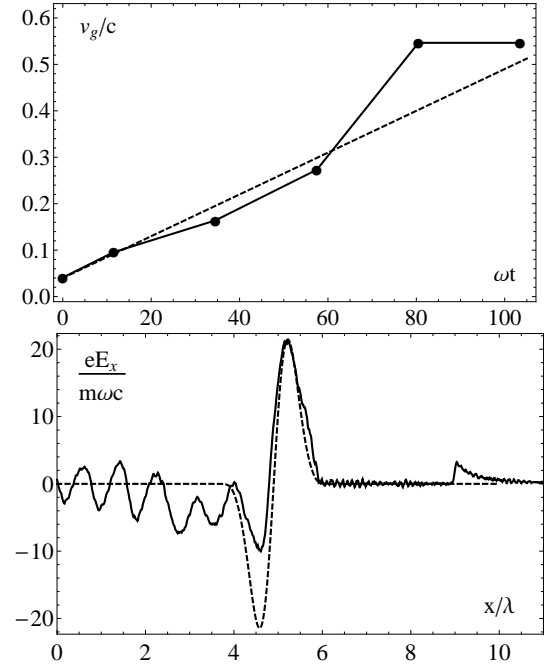


FIG. 5. Pulse velocity inside a $6\text{ }\mu\text{m}$ target with an electron density $20n_c$ for a laser pulse with an energy of 30 J (top panel) and an electrostatic field (bottom panel). The target is placed from $x = 3\lambda$ to $x = 9\lambda$. The dashed curve corresponds to the Gaussian fit of the potential.

result of the SASL mechanism. We estimated the energy gain of the test protons (initially at rest or weakly pre-accelerated) in the electrostatic field shown by the dashed curve in Fig. 5 as the solution of system (1). At the distance of $6\text{ }\mu\text{m}$, the protons gain energy of 350 to 400 MeV (see Fig. 6), which is consistent with the PIC simulation result. For $x > 6\lambda$, the electrostatic potential overtakes the protons and decelerates them as a result of the transition to the relativistic regime and violation of the phasing-in.

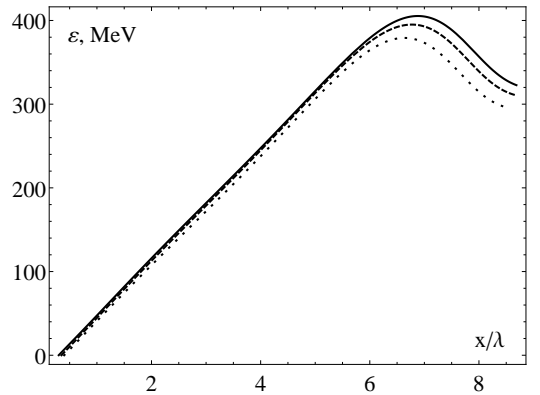


FIG. 6. Energy gain of test protons with $x_0 = 0.4\lambda$ and $p_0 = 0$ (dotted curve), $x_0 = 0.3\lambda$ and $p_0 = 0.01$ ($E_0 = 50\text{ keV}$) (solid curve), and $x_0 = 0.35\lambda$ and $p_0 = 0$ (dashed curve).

In conclusion, we have proposed a new model of proton acceleration by an ultraintense slow light pulse interacting with low-density targets. The key points of this mechanism are to stop the laser pulse at the front of the target and then accelerate the infiltrating intense part of the pulse inside a plasma at the same rate as the proton energy increase in a ponderomotive potential to achieve synchronized acceleration by slow light (SASL). In the case considered, the linearly polarized laser pulse propagates and increases its group velocity as a result of a relativistic self-induced transparency. Another scheme of pulse acceleration could be based on using a plane target with its density decreasing from front to back. The SASL regime is challenging for low-density material applications and will require production of lightweight foils with fully variable and controllable parameters. Such foils should typically have a multimicron thickness that makes them more robust in laser acceleration experiments in contrast to nanoscale solid dense foils, which require an extremely high intensity contrast ratio. Finally, we note that our simulations with low-density targets have demonstrated more than a twofold increase of proton energy compared with the increase in the case of solid dense foils of optimal submicron thickness [24].

This research was funded by a grant from the Russian Science Foundation (Project No. 14-12-00194).

-
- [1] H. Daido, M. Nishiuchi, and A. S. Pirozhkov, *Rep. Prog. Phys.* **75**, 056401 (2012).
 - [2] A. Macchi, M. Borghesi, and M. Passoni, *Rev. Mod. Phys.* **85**, 751 (2013).
 - [3] M. Passoni, A. Zani, A. Sgattoni, D. Dellasega, A. Macchi, I. Prencipe, V. Floquet, P. Martin, T. V. Liseykina, and T. Ceccotti, *Plasma Phys. Control. Fusion* **56**, 045001 (2014).
 - [4] J. H. Bin, W. J. Ma, H. Y. Wang, M. J. V. Streeter, C. Kreuzer, D. Kiefer, M. Yeung, S. Cousens, P. S. Foster, B. Dromey, et al., *Phys. Rev. Lett.* **115**, 064801 (2015).
 - [5] O. Shorokhov and A. Pukhov, *Laser Part. Beams* **22**, 175 (2004).
 - [6] B. Shen, Y. Li, M. Yu, and J. Cary, *Phys. Rev. E* **76**, 055402 (2007).
 - [7] E. Esarey, C. Schroeder, and W. Leemans, *Rev. Mod. Phys.* **81**, 1229 (2009).
 - [8] A. Pukhov and J. Meyer-ter Vehn, *Appl. Phys. B* **74**, 355 (2002).
 - [9] B. Shen, X. Zhang, Z. Sheng, M. Y. Yu, and J. Cary, *Phys. Rev. ST Accel. Beams* **12**, 121301 (2009).
 - [10] L.-L. Yu, H. Xu, W.-M. Wang, Z.-M. Sheng, B.-F. Shen, W. Yu, and J. Zhang, *New J. Phys.* **12**, 045021 (2010).
 - [11] X. Zhang, B. Shen, L. Ji, F. Wang, M. Wen, W. Wang, J. Xu, and Y. Yu, *Phys. Plasmas* **17**, 123102 (2010).
 - [12] F. L. Zheng, S. Z. Wu, C. T. Zhou, H. Y. Wang, X. Q. Yan, and X. T. He, *Europhys. Lett.* **95**, 055005 (2011).
 - [13] T. Esirkepov, M. Borghesi, S. Bulanov, G. Mourou, and T. Tajima, *Phys. Rev. Lett.* **92**, 175003 (2004).
 - [14] A. A. Saha, F. S. Tsung, A. R. Tableman, W. B. Mori, and T. C. Katsouleas, *Phys. Rev. E* **88**, 043105 (2013).
 - [15] H. Y. Wang, X. Q. Yan, and M. Zepf, *Phys. Rev. ST Accel. Beams* **18**, 021302 (2015).
 - [16] D. Haberberger, S. Tochitsky, F. Fiuza, C. Gong, R. A. Fonseca, L. O. Silva, W. B. Mori, and C. Joshi, *Nat. Phys.* **8**, 95 (2011).
 - [17] C. K. Lau, P. C. Yeh, O. Luk, J. McClenaghan, T. Ebisuzaki, and T. Tajima, *Phys. Rev. ST Accel. Beams* **18**, 024401 (2015).
 - [18] T. Katsouleas, *Phys. Rev. A* **33**, 2056 (1986).
 - [19] S. V. Bulanov, E. Y. Echkina, T. Z. Esirkepov, I. N. Inovenkov, M. Kando, F. Pegoraro, and G. Korn, *Phys. Rev. Lett.* **104**, 135003 (2010).
 - [20] F. Cattani, A. Kim, D. Anderson, and M. Lisak, *Phys. Rev. E* **62**, 1234 (2000).
 - [21] E. Siminos, M. Grech, S. Skupin, T. Schlegel, and V. T. Tikhonchuk, *Phys. Rev. E* **86**, 056404 (2012).
 - [22] R. Z. Sagdeev, "Cooperative Phenomena and Shock Waves in Collisionless Plasmas", ed. by M.A. Leontovich in *Reviews of Plasma Physics*, Vol. 4. Consultants Bureau, New York, 1966, p.23
 - [23] D. V. Romanov, V. Y. Bychenkov, W. Rozmus, C. E. Capjack, and R. Fedosejevs, *Phys. Rev. Lett.* **93**, 215004 (2004).
 - [24] A. V. Brantov, E. A. Govras, V. Y. Bychenkov, and W. Rozmus, *Phys. Rev. ST Accel. Beams* **18**, 021301 (2015).